Journal of Materials Chemistry A

Sub-Monolayer Control of the Growth of Oxide Films on Mesoporous Materials

Journal:	*Journal of Materials Chemistry A*
Manuscript ID	TA-ART-06-2018-005431.R1
Article Type:	Paper
Date Submitted by the Author:	15-Aug-2018

Complete List of Authors:	Weng, Zhihuan; Dalian University of Technology, Department of polymer science & Engineering Chen, Zhihui; Changzhou University, School of Materials Science and Engineering, Jiangsu Collaborative Innovation Center of Photovolatic Science and Engineering Qin, Xiangdong; University of California, Chemistry Zaera, Francisco; University of California, Chemistry

Sub-Monolayer Control of the Growth of Oxide Films on Mesoporous Materials

Zhihuan Weng,[§] Zhi-hui Chen,[‡] Xiangdong Qin, and Francisco Zaera*

Department of Chemistry and UCR Center for Catalysis, University of California, Riverside, CA 92521, USA

*Email: zaera@ucr.edu

Abstract

The use of atomic layer deposition (ALD) as a way to deposit good-quality oxide films on the inside surfaces of mesoporous materials in a controlled fashion was explored for a number of systems, combining SBA-15, MCM-41, FDU-12 materials and spherical mesoporous silica particles (SMSP) with Al_2O_3, TiO_2, and SiO_2 films. Advantage was taken of the well-defined nature of the pores in most of those materials to use N_2 adsorption-desorption isotherms as a way to characterize the deposition process. It was seen that while the average size of the pores decreases monotonically with the number of ALD cycles used (because of the newly deposited layers), their size distribution remains as narrow as in the original samples, an observation that attests to the even coverage of the surfaces in a layer-by-layer fashion. This was confirmed

[§] Present Address: Department of Polymer Science & Engineering, Dalian University of Technology, Dalian 116024, People's Republic of China

[‡] Present Address: School of Materials Science and Engineering, Changzhou University, Changzhou, 213164, Jiangsu, China

further by transmission electron microscopy. Additional measurements of pore volumes and surface areas were used to further evaluate the effectiveness of the ALD processes. It was found that excessive exposures of the solids to the precursors during each ALD cycle lead to condensation at the bottom of the pores and to subsequent pore plugging, whereas insufficient doses prevent full coverage of the surfaces, leaving the original silica in the back of the pores exposed. These problems can be minimized by tuning the process parameters, but become more acute with small-pore samples such as MCM-41 or SMSP. With samples having large pores connected via small windows (FDU-12), film growth takes place inside the pores without affecting the size of the windows. Finally, the deposition of silicon oxide films is much slower than that of the other oxides, but can still be achieved using a modified experimental setup.

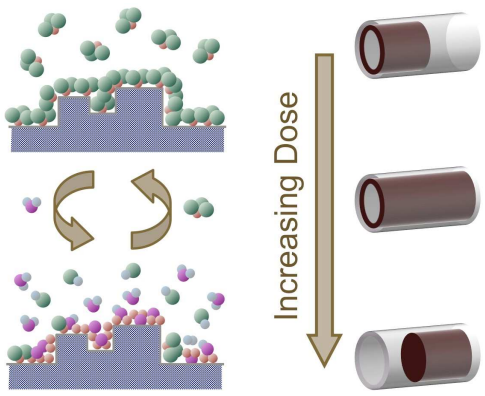

1. Introduction

Because of its versatility and wide range of uses, the deposition of thin solid films by chemical means has received ample attention by the research community in recent years. Atomic layer deposition (ALD), by which the chemical reactions involved are split into two or more self-limiting and temporarily-separate steps, is a particularly appealing approach that offers great control of film thickness with minimum restrictions in terms of process conditions.[1-4] One of the most promising characteristics of chemical vapor deposition (CVD) and ALD processes is their isotropy, a property that affords the even deposition of films conformally on topographically challenging surfaces.

For many years, research on ALD has been dominated by its application in microelectronics fabrication and related technologies.[5-9] Although the initial substrates in microelectronic fabrication are typically flat silicon wafers, those surfaces become increasingly rougher as layers of different materials are added in order to develop the individual microelectronic components (transistors, capacitors, etc.) and to electrically connect them to attain the final desired circuit. The increasing complexity of the microelectronic circuits in modern devices has led to the need to deposit thin films on structures with aspect (depth to width) ratios of up to a 100, within dimensions on the order of few tens of nanometers. Nevertheless, as challenging as that has become, in particular since the microelectronic industry often relies on physical, evaporation-based and directional deposition methods, the difficulties with film depositions in microelectronics do not compare with the stringent requirements associated with the coating of mesoporous materials, which commonly comprise nanometer-size pores with length of up to

several micrometers. The use of ALD has in recent years been extended to many new applications, including catalysis, sensoring, membranes, sorbents, solar and fuel cells, batteries, and photovoltaics, which involve such solids with mesoporous structures.[10-14] Even for chemical deposition methods, film growth on those is often problematic, and requires process optimization to avoid side reaction, undesirable nucleation of discrete nanoparticles, and/or condensation and other mass transport bottlenecks.[15]

Only limited research has been directed at understanding and designing CVD and ALD processes for mesoporous materials. Those processes are often limited by Knudsen diffusion, a phenomenon that has been modeled from a theoretical/computational point of view.[16-18] Gradients in surface coverage as a function of pore depth have been identified during the dosing of ALD precursors,[19,20] a result that can lead to uneven film growth. However, the specifics of these profiles and the consequences in terms of process design have proven to be quite complex, depending on many interconnected parameters, and therefore hard to predict based on engineering rules alone;[21] it may be that the conditions in ALD need to be set empirically for each individual system. A general assessment of the performance of ALD processes on mesoporous materials, the identification of the key parameters affecting the quality of the resulting films, and the development of probing procedures to help with those evaluations, are needed.

Here, we report results from our study on the ALD of oxide films on oxide supports with mesoporous structures. Specifically, we explore the conditions required to deposit Al_2O_3, TiO_2, and SiO_2 thin films on the walls of the pores of SBA-15, MCM-41 and FDU-12 mesoporous

solids as well as on spherical mesoporous silica particles (SMSP). The quality of the deposited films was characterized primarily via the analysis of N_2 adsorption-desorption isotherms, taking advantage of the fact that, because of the uniformity of the pore dimensions in these materials, the pore size distributions are narrow and well defined.[22-25] The use of mesoporous materials with well-defined pore structures is critical in these studies, because adsorption-desorption experiments on other porous solids yield wide pore size distributions and do not afford the ability to evaluate the film thickness of the deposited films.[26,27] It was found that the uniformity of the films does indeed depend critically on the deposition conditions: insufficient dosing of the ALD precursors leads to preferential deposition near the entrance of the pores, whereas excessive dosing results in condensation and in the plugging of the bottom of the pores. On the other hand, upon proper tuning, the ALD method proved quite versatile, being applicable to the growth of many oxide films and on many mesoporous materials. We envision ALD becoming a powerful tool for the manufacturing of unique mesoporous materials with mixed-oxide structures for specific uses in catalysis and other fields,[28-34] and the adsorption-desorption evaluating approach exposed here a way to easily tune the process parameters for those applications.

2. Experimental Details

2.1. ALD Reactor. The film-deposition experiments were carried out in a homemade ALD reactor made out of a six-way stainless steel cross sealed with 2¾" Conflat flanges. The main reaction chamber can be heated to temperatures of up to 400 K by using a set of heating tapes wrapped around its outside. The powder sample is placed in a holder consisting of a 3 x 2 cm^2

shallow tray, ~ 5 mm deep, made out of a Ni sheet. This holder can be heated resistively by passing current through appropriate feedthroughs connected to a pair of supporting Ni wires. The powder is spread on the tray to form a layer approximately 1 mm in depth, and covered with a tightly fitted lid made out of a stainless steel wire mesh to hold it in place and prevent it from being blown away during pumping and purging. The temperature of the sample holder is monitored with a K-type thermocouple wire pair spotwelded to the backside of the tray, and set independently from that of the chamber by using a separate controller. Powder samples can be heated with this arrangement to temperatures of up to 625 K during the depositions.

Two independent precursor and purging gas delivery lines are attached to two of the flanges bolted to the reaction chamber. Gas-phase precursors, liquid precursors with high vapor pressures, and purging gases (either Ar or N_2) are all fed to the system directly, whereas precursors with low vapor pressures are delivered using a bubbler. Separate gas lines with appropriate valves to the chamber and to the pumping system are set up for each of the two main chemicals used in a given ALD experiment. The reactor can be evacuated using a mechanical pump connected to the six-way cross via a 1½" right-angle valve, and typically reaches ultimate pressures around or below 5 mTorr, as measured by a thermocouple gauge. In a typical ALD cycle, the chemicals are fed into the chamber in sequence, with purging cycles performed in between, while maintaining continuous pumping.

2.2. Aluminum Oxide and Titanium Oxide ALD. The deposition of Al_2O_3 films was carried out by alternating dosings of TMA (trimethylaluminum(III), Aldrich-Sigma, >97% purity) and deionized water, following well-documented chemistry.[35-38] The powder sample (SBA-15 or any

of the other mesoporous materials; ~ 40 mg) was first heated under vacuum at 475 K for 2 h in the holder's tray to remove all physisorbed moisture. After that, the TMA, held in a stainless-steel reservoir at room temperature, was introduced as a vapor into the chamber at a pressure of 200 mTorr (without carrier gas) and flowed for a set time (indicated in the corresponding figures). The rector was then flushed with argon at 500 mTorr for a fixed time, and deionized water, held in a glass tube with a bubbler, was injected into to reactor at a pressure of 200 mTorr. Following the water dosing, the chamber was flushed with argon a second time. These cycles were repeated as needed before extracting the solid powder for analysis. Typical time sequences in these Al_2O_3 ALD cycles were TMA:Ar:H_2O:Ar = 120s:300s:120s:600s, and the deposition was carried out at 475 K unless otherwise indicated.

TiO_2 films were deposited using ALD cycles with TDMAT (tetrakis(dimethylamido)Ti(IV), Aldrich-Sigma, 99.999% purity –trace metals basis–) and deionized water, following chemistry also amply studied and characterized in the literature.[39-42] Typical cycle times were TDMAT:N_2:H_2O:N_2 = 20min:50min:2min:50min, and the depositions were normally carried out at 375 K, the same for both the sample and the reactor; the precursor was kept at 315 K. It is worth noticing that the gas exposures in these titanium oxide ALD cycles are much longer than those used for aluminum oxide deposition, as the TDMAT precursors is much less volatile and reactive than TMA, and because the TiO_2 deposition was carried out at lower temperatures.

2.3. Silicon Oxide ALD. The deposition of silicon oxide films is more difficult than that of other oxides, because the precursors used in this case tend to exhibit moderate to low reactivity. Silica deposition in either liquid phase or CVD often relies on the reaction of tetramethylorthosilicate

(TMOS) or tetraethylorthosilicate (TEOS) and water,[43] and the same chemistry can be harvested to design ALD processes. However, our attempts to deposit SiO_2 films with TMOS (Aldrich-Sigma, ≥99% purity) and deionized water using our ALD reactor failed, even if using temperatures as high as 575 K and dosings of up to 20 min.

Instead, an alternative protocol was employed based on the static exposure of the powders to an atmosphere of the ALD reactants, as described in the literature.[44] In our setup, a vial (8 ml volume) containing the solid sample (~ 30 mg of SBA-15, for instance) was attached to a metal wire and suspended inside a round-bottom flask approximately 1 cm above the liquid, which consisted of 0.4 ml TMOS. The flask was partly immersed in an oil bath held at 355 K so that the solid sample could be exposed to the TMOS vapor for several minutes while stirring. After this exposure, the vial with the powder was moved to a two-neck flask, and the system was pumped. Next, the sample in the vial was exposed to a mixture of water and ammonia vapors (the latter used as a catalyst)[45,46] at room temperature in another round-bottom flask for several minutes while stirring. This was followed by a second round of pumping. Such ALD cycle was repeated as needed.

2.4. Mesoporous Materials. All three mesoporous materials with well-defined pore structures used here, namely, SBA-15 (Sigma-Aldrich, ≥ 99.9% SiO_2 purity, surface area = 700 ± 50 m^2/g, pore volume = 0.5 – 0.7 cm^3/g, pore diameter > 6 nm), MCM-41 (Sigma-Aldrich, surface area = ~ 1000 m^2/g, pore volume = 0.98 cm^3/g, pore diameter = 2.1 – 2.7 nm), and FDU-12 (ACS Materials, ≥ 99% SiO_2 purity, surface area = 600 m^2/g, pore volume = 0.66 cm^3/g, pore diameter > 10 nm, pore entrance = 3.8 nm), were purchased from commercial sources and used as

supplied.

The spherical mesoporous silica particles (SMSP) were prepared by following a recipe from the literature:[47] (1) 1.75 mL of NaOH (2.0 M) was added into a solution of cetyltrimethylammonium bromide (CTAB, 0.5 g, 1.37 mmol; Sigma Aldrich, ≥ 98% purity) in deionized water (240 mL) while stirring; (2) the temperature of the mixture was increased to 355 K; (3) 2.7 g of tetraethyl orthosilicate (TEOS, 13.0 mmol; Sigma-Aldrich, ≥9 9% purity) was added; (4) the mixture was stirred for 2 h at 355 K; (5) the precipitate was collected by filtration, washed with deionized water and methanol, and dried under vacuum at 315 K overnight; and (6) the resulting solid was calcined at 825 K in air for 5 h to remove the CTAB surfactant.

2.5. Characterization of the Solids. Adsorption-desorption isotherm measurements were carried out in a NOVA@2000e gas sorption system, using N_2 as the adsorbent. Data analysis was carried by using the Nova Win software: pore distributions and total pore volumes were estimated using the BJH (Barrett-Joyner-Halenda) equations[48] for Type IV isotherms,[49] whereas total surface areas were calculated by using the BET (Brunauer-Emmett-Teller) isotherm.[50] Transmission electron microscopy (TEM) images were obtained using a Philips Tecnai 12 instrument (120 kV accelerating voltage).

3. Results and Discussion

The quality of the oxide films grown by ALD was probed mainly via the analysis of N_2

adsorption-desorption isotherms. Thanks to the well-defined and simple structure of the pores in the mesoporous solids used here, that analysis provided a wealth of information about the homogeneity and thickness of the films. In particular, because SBA-15 and MCM-41 are silicon oxide-based materials with one-dimensional cylindrical pores of constant diameter, the homogeneous deposition of thin films on the surface of those pores is manifested by a discrete reduction in pore diameter. The quality of those films can be assessed by the spread of the pore size distribution, whereas the extent of the deposition can be evaluated by comparing the measured values for total volume and total area against those estimated assuming cylindrical pores.

To illustrate our procedure, we first report in Figure 1 typical N_2 adsorption-desorption isotherms obtained from SBA-15 samples modified via the deposition of films of either aluminum oxide (left panel) or titanium oxide (right) of various thickness (that is, after different numbers of ALD cycles). The shapes of these isotherms are all typical of what the IUPAC classification denotes as Type IV, which display an initial monolayer saturation followed by multilayer adsorption and capillary condensation.[49] A characteristic hysteresis is also seen between the adsorption and desorption branches of the isotherms with a shape of the H1 type (again, according to the IUPAC nomenclature), reflecting the differences in the onsets for condensation (adsorption branch) versus evaporation (desorption branch): the meniscus radius associated with the latter is half of that associated with the former, and that leads to evaporation at lower pressures than those needed for condensation.

The isotherms in Figure 1 exhibit, qualitatively at least, the expected trends from ALD

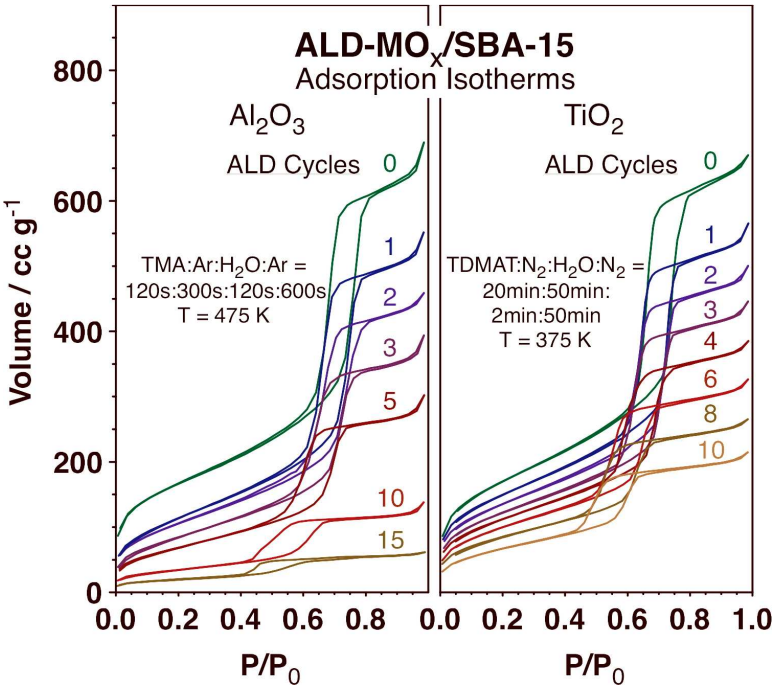

Figure 1. N_2 adsorption-desorption isotherms, in the form of uptake volume versus pressure, for SBA-15 samples on which either aluminum oxide (left panel) or titanium oxide (right) thin films have been deposited by ALD. Data are reported as a function of the number of ALD cycles used.

modification of the SBA-15 pores. Specifically, the total amount of nitrogen consumed (that is, the total absorbed volume), which is determined by the value at $P/P_0 = 1$, decreases with the number of ALD cycles used. This indicates that the deposited films reduce the empty volume inside the pores, more the more ALD cycles are carried out. Also to note is the shift of the hysteresis loop toward lower pressures with increasing number of ALD cycles: condensation occurs at lower pressures because the pores are smaller. Finally, the shape (if not the size) of the hysteresis loop is not affected by the film deposition, suggesting that the geometry of the pores is not been greatly changed from its original cylindrical geometry. All these trends are clearly seen for both cases reported here, for the deposition of either aluminum oxide or titanium oxide on SBA-15.

The adsorption-desorption isotherms can be processed using the equations derived by Barrett, Joyner and Halenda (BJH) to extract pore size distributions.[48] The results from such analysis are shown in Figure 2 for the case of the aluminum oxide films. Two sets of data are reported there, calculated from the adsorption (left panel) and desorption (right) branches, respectively. Although the qualitative trends are similar in both cases, the values for the pore diameter estimated in each case are different. This is a typical result, and the reasons for it have been discussed extensively in the literature already.[49] For cylindrical pores such as those in SBA-15,

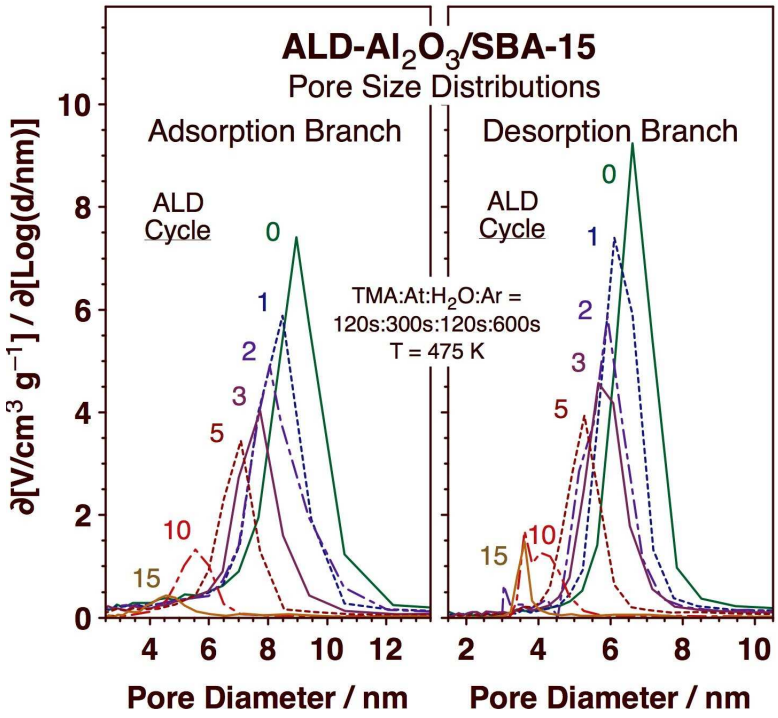

Figure 2. Pore size distributions for SBA-15 samples onto which aluminum oxide films have been grown as a function of the number of ALD cycles used. Data are shown from calculations using the BJH equation on the adsorption (left panel) and desorption (right) branches of the isotherms reported in Figure 1. The pore diameter is reduced with increasing number of ALD cycles while the narrow pore size distribution typical of the SBA-15 material is retained.

it is suggested that the data from the desorption branch may better represent the actual pore diameters, as they correspond to an equilibrium situation. What are perhaps the more relevant observations here are that: (1) the average pore diameters decrease monotonically with the number of ALD cycles; and (2) the size distributions are relatively sharp, a reflection of the uniformity of the pore sizes within the whole sample and of their cylindrical geometry. It is particularly noteworthy that the same type of narrow pore size distributions is seen in the ALD-treated samples, even after 10-15 cycles (which leads to a reduction in pore diameter to approximately half). This result points to the conformal and homogeneous nature of the deposited films.

Figure 3 summarizes the geometrical parameters extracted from the analysis of the adsorption-desorption isotherms for the case of the Al_2O_3-ALD SBA-15 samples. The left panel shows the pore diameters calculated in three different ways, by using the BJH equation on the adsorption (red open circles) and desorption (blue solid squares) branches of the isotherms, and by using the measured total pore volumes (V) and total surface areas (A) assuming a cylindrical pore shape (green solid diamonds). Nice linear trends are seen in the first two cases for the pore diameters as a function of the number of ALD cycles, indicating the layer-by-layer growth of the films. A constant deposition rate of approximately 1.4 Å/cycle was estimated from these data, comparable (albeit a bit higher) to those reported for other surfaces and systems.[24,35,51] Also to note is the fact that the two curves, for the adsorption and desorption branches, are offset by approximately 2 nm, the former yielding the higher pore diameter values. As mentioned above, it is believed that the numbers from the desorption branch better reflect reality, a fact corroborated here by electron microscopy (TEM) images such as those in Figure 4, obtained for the same samples; the

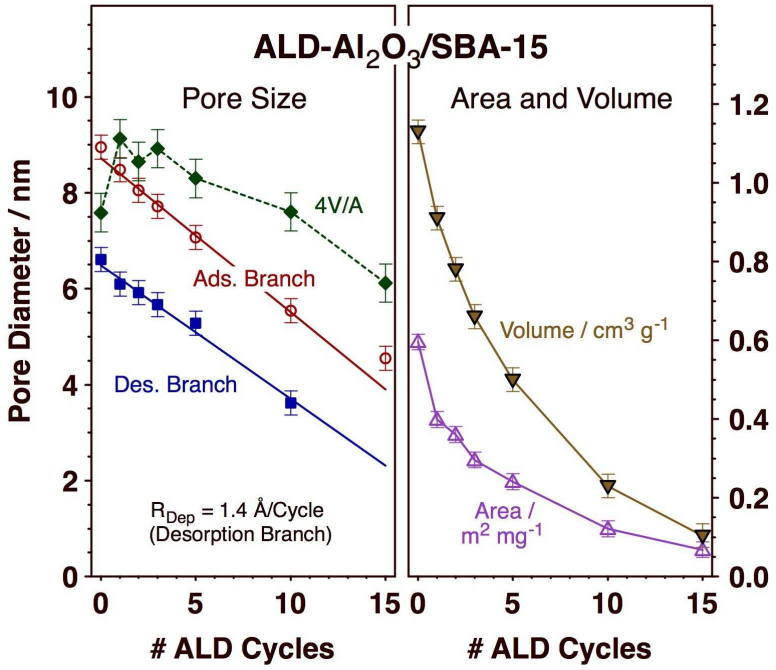

Figure 3. Summary of the geometrical dimensions of the pores of the SBA-15 samples treated with various numbers of Al_2O_3 ALD cycles. Left: Average pore diameters, estimated from the adsorption and desorption branches of the isotherms in Figure 1 (the peaks in the distributions in Figure 2), and from the volume-to-area ratio of the pores assuming a cylindrical shape. A linear decrease in pore size is seen with the number of ALD cycles, for a deposition rate of approximately 1.4 Å/cycle. Right: Trends for the total pore volumes and for the total surface areas.

data in that figure correspond to a clean SBA-15 sample (left panel) and to a solid treated with 5 Al_2O_3 ALD cycles. The total pore structure, including the walls, is estimated from the TEM images to be approximately 7 nm in diameter. In the case of the pure SBA-15, the pore opening is calculated at approximately 5.4 nm, whereas in the sample coated with aluminum oxide the opening is only about 3.3 nm in diameter; the values extracted from the desorption isotherm are 6.6 and 4.5 nm, respectively.

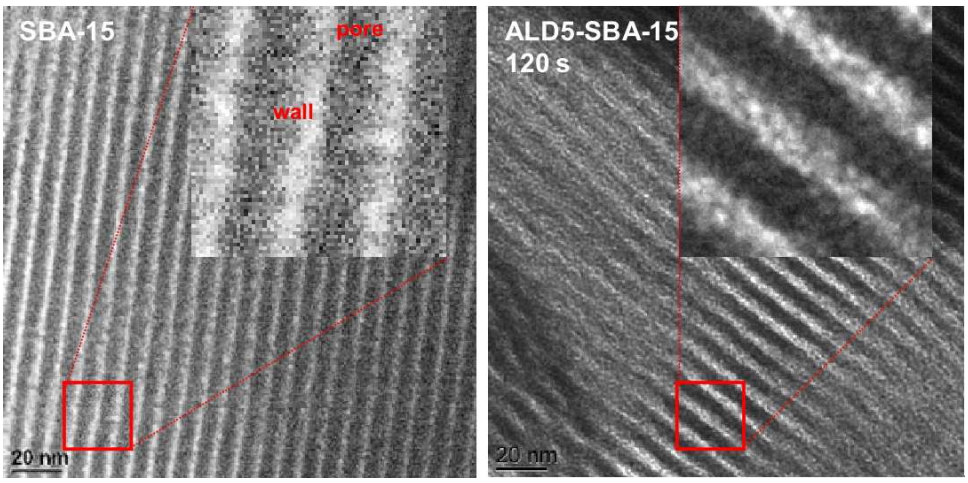

Figure 4. Transmission electron microscopy (TEM) images for SBA-15 samples, pristine (left panel) and after 5 Al_2O_3 ALD cycles (right). The pore sizes determined from these images are consistent with those estimated from the desorption isotherms.

The values of the pore diameters estimated using the volume-to-area ratios (4V/A, assuming a cylindrical shape) are somewhat higher than those extracted directly from the pore size distributions, and also show a less smooth trend. This discrepancy can be explained by a number of factors. For one, the 4V/A ratio is calculated from volume and area global values, integrated over the whole sample. This is likely to include regions with defects and with pores of lesser quality. In addition, the trends measured independently for V and A as a function of the number of ALD cycles, reported in the right panel of Figure 3 (golden solid down-pointing triangles and pink open up-pointing triangles, respectively), display themselves some deviations from their expected behavior. In particular, for perfect cylinders the surface area should scale linearly with film thickness, and that is not the case here: a sharper drop in pore diameter is seen in the first few ALD cycles instead. Perhaps the adsorption isotherms do not accurately measure the real pore diameter, as the surface after the ALD cycles are likely to be terminated by either hydroxo or methyl groups, and those may make the pores appear smaller than they really are. This

behavior may change as the surface transitions from silicon oxide to aluminum oxide termination, leading to a slower decrease in pore diameter per ALD cycle in the later depositions. It should be mentioned that similar changes in apparent film thickness evolution with ALD cycle have been reported for other systems in the past.[24,52] Interestingly, the total pore volume with ALD cycle (and film thickness) follows a dependence close to the square of the pore diameter, the behavior expected for cylindrical pores.

There is another possible explanation for the deviations in total pore volume and total surface area reported above, and that is that the deposition during the ALD cycles may not be homogeneous after all. In particular, it is possible for the TMA ALD precursor to condense inside the pores. It is worth remembering that, as the adsorption-desorption isotherms in Figure 1 indicate, condensation inside the pores starts at a fraction (about half) of the saturation pressure. If too much TMA is dosed in the first half of the ALD cycles, and/or if that TMA is not properly flushed away in the intermediate stages of those cycles, the liquid can react with water in the second half and plug the back end of the pores. This hypothesis was tested and corroborated by carrying out ALD experiments using shorter TMA exposures. As shown in Figure 5, such change led to increases in both pore volume and surface area without affecting the average pore diameter. Specifically, after 2 ALD cycles, the volume and area values obtained with 120 s TMA exposures, 0.75 cm^3/g and 0.410 m^2/mg, respectively, increased to 0.96 cm^3/g and 0.525 m^2/mg, if the dose is reduced to 60 s or less; while the pore diameter remained at 6.3 ± 0.1 nm all throughout. It is clear that there is a need to avoid excessive exposures of the solids to the ALD precursors if pore plugging is to be avoided.

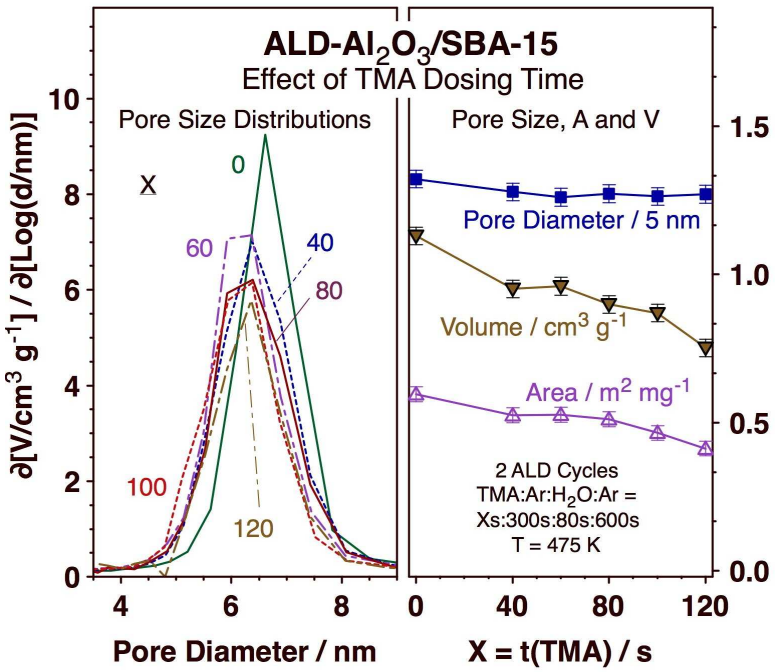

Figure 5. Pore size distributions (left panel) and average pore diameters, total pore volumes, and total surface areas (right) for SBA-15 samples treated with two Al_2O_3 ALD cycles as a function of the time of exposure to TMA used. Shorter exposures lead to higher volumes and areas without changing the pore diameters, a result that suggests less pore plugging.

There is, however, a limit to how short of an exposure can be used in the ALD process to obtain complete pore coverage; too short of a pulse, and the deep end of the pores may not be properly exposed to the precursor and consequently may not be covered with any new oxide film. This problem is illustrated by the data in Figure 6, which correspond to titanium oxide ALD experiments on SBA-15 carried out under the conditions listed in Table 1. The left panel of that figure shows the pore size distributions measured for five samples on which TiO_2 films were deposited following 8 ALD cycles with various exposure and pumping times. The data have been arranged in order, from bottom to top, of increasing exposures, except for the transition from Sample B to Sample C, where the mass of the catalyst used was reduced instead. A

bimodal distribution is seen in most cases, with peaks at 4.49 and 6.35 nm; the latter corresponds to the pore diameter of pure SBA-15, whereas the former is the diameter expected from pores with walls covered with the TiO_2 deposited by ALD (assuming a deposition rate of ~ 1.1 Å/cycle). Our results indicate that, in general, short TDMAT exposures may lead to incomplete coating of the pores, and that the extent of the pore surfaces covered by ALD increases with increasing dosing times. We speculate that only the front of the pores, the region nearest to the pore entrance, receives enough ALD precursor to deposit titania on the surface, whereas the back is prevented from being exposed to any precursor at all if not enough time is allowed for complete diffusion to take place. The fractions of uncovered and TiO_2-covered areas obtained in each case are reported on the right panel of Figure 6, together with the data for the pore volumes and surface areas, which also decrease with the extent of the ALD coverage. It is worth mentioning here that, although adsorption-desorption isotherms have been used in the past to follow ALD processes,[23,37,53-55] this is the first instance where, to the best of our knowledge, a detailed analysis of the data has been used to evaluate their performance and the quality of the resulting films. In particular, we are not aware of any other report of bimodal pore size distributions resulting from incomplete ALD as those shown in Figure 6.

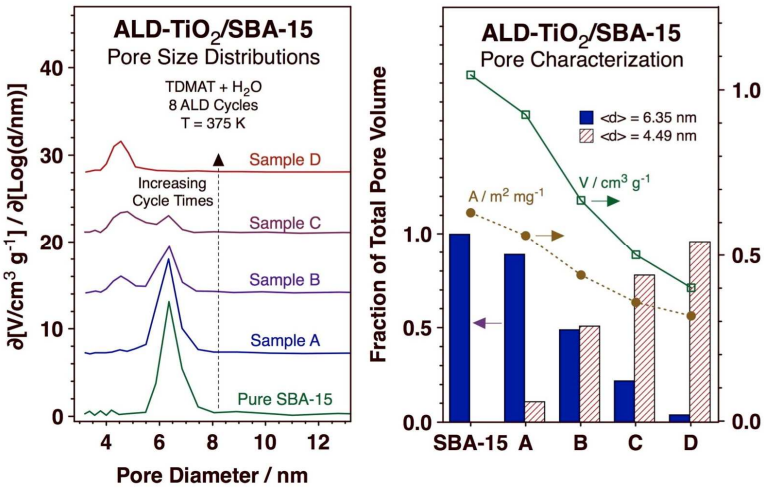

Figure 6. Left: Pore size distributions obtained from adsorption-desorption isotherms measured on five samples treated with 8 TiO_2 ALD cycles. The results are in general ordered in terms of increasing TDMAT and H_2O exposures (the specific conditions for each case are listed in Table 1). It is clearly seen that after short exposures bimodal pore size distributions are obtained, indicative of incomplete pore coverage. Right: Calculated fractions of uncovered and TiO_2 covered surfaces for the samples in Table 1, as estimated from the data in the left panel, together with the values for the total pore volumes and total surface areas.

Table 1. TiO_2 ALD parameters for the preparation of the samples reported in Figure 6.

Sample	mass / mg	t(TDMAT) / s	$t(N_2)$ / s	$t(H_2O)$/ s	$t(N_2)$ / s
Pure SBA-15	5	0	0	0	0
A	55	5	100	5	100
B	55	120	600	20	600
C	16	120	600	20	600
D	5	600	1800	60	1800

Other parameters can also affect the effectiveness of the ALD processes with mesoporous

materials. In Figure 7, data are shown to illustrate the effects of water dosing (left panel) and sample temperature (right) for the case of Al_2O_3 ALD on SBA-15. In terms of water dosage, the data show that, perhaps counterintuitively, the use of higher water doses (and shorter purging times afterward) in the ALD cycles leads to samples with larger (not smaller) surface areas. Interestingly, this increase in area is not accompanied by any significant changes in pore diameter or (more puzzling) pore volume. We explain this behavior by suggesting that perhaps after high H_2O doses water may condense on the outside interstitial spaces in between SBA-15 nanoparticles, facilitating the growth of alumina layers via CVD leading to the fusing of the separate particles. This may not be desirable, so we conclude that limited water exposures and

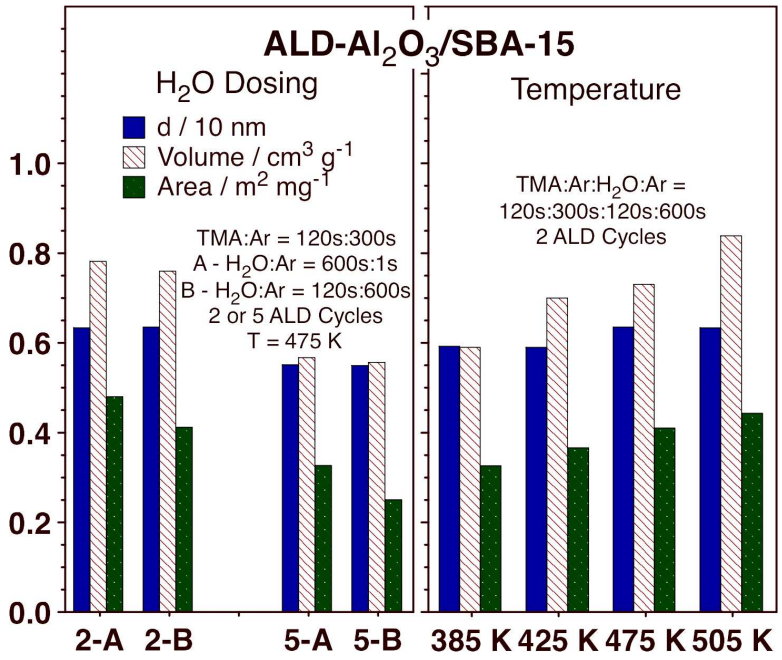

Figure 7. Pore geometrical data, calculated from N_2 adsorption-desorption isotherms, for SBA-15 samples treated with aluminum oxide ALD versus water dosing times (left panel) and sample temperature (right). Reported are the average pore diameters, total pore volumes, and total surface areas. It is concluded that low water doses, long purging times, and high deposition temperatures are best.

large purging times afterward may be better for the homogeneous growth of the ALD films, at least within the time ranges reported here (and in connection with our reactor; the dosing and purging times are expected to depend heavily on the particulars of the reactor and process used). In terms of substrate temperature (Figure 7, right panel), the data indicate that higher temperatures lead to samples with higher surface areas and larger pore volumes. These trends are not accompanied by any significant increases in pore diameter, which means that they likely reflect a better deposition process, with minimal pore plugging due to precursor condensation. Another possibility is that higher reaction temperatures may facilitate the deposition of higher density films. Within the temperature range explored in this work (up to 505 K), higher temperatures may be better for ALD film growth.

Figure 8 reports representative data from studies on the deposition of silicon oxide films on SBA-15 by using TMOS + $NH_3 \cdot H_2O$ ALD. As discussed already in the Experimental section, the chemistry used for silicon oxide film growth is slower and much less effective than that used for aluminum oxide or titanium oxide depositions. A different experimental setup was required to optimize the exposures of the solid samples to the silicon precursors, but even with the new approach, it was found that SiO_2 deposition on the pores of SBA-15 is quite slow. The left panel of Figure 8 shows the pore size distributions obtained for representative cases. It is seen there that even after 9 ALD cycles the pore diameter was reduced to only about 6.4 Å, implying an average deposition rate of ~ 0.35 Å/cycle. Surprisingly, increasing TMOS exposure times leads to increases in total pore volume and total surface area without affecting the pore size (Figure 8, center panel), a desirable if counterintuitive trend. The ammonia dosing time, on the other hand, appears to have minimal effect on the quality of the deposited films, at least within the time

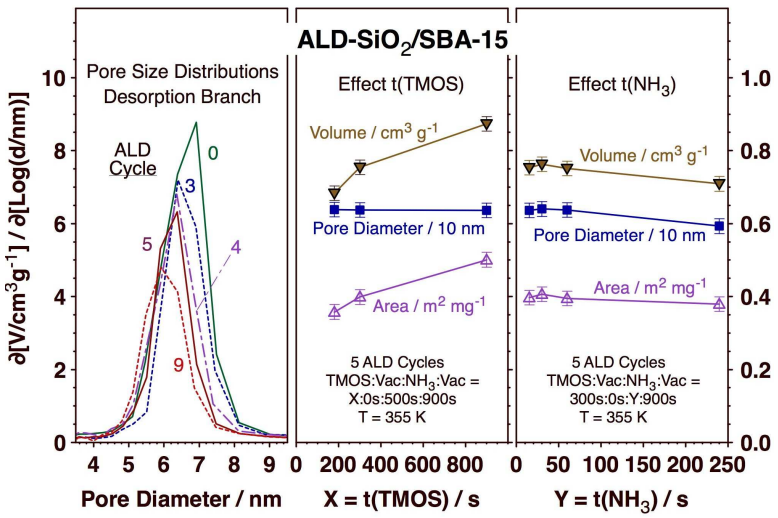

Figure 8. Characterization data for solids made out of depositing SiO_2 films on SBA-15 via TMOS + $NH_3 \cdot H_2O$ ALD cycles. Left: Typical pore size distributions versus the number of ALD cycles used. Center: Pore diameter, total pore volume, and total surface area versus TMOS exposure time. Right: Pore diameter, total pore volume, and total surface area versus ammonia + water exposure time. Controlled, albeit slow, silicon oxide film growth is possible using the alternative ALD setup described in this report.

range tested here (Figure 8, right panel). The good news is that good-quality silicon oxide films can be deposited in a controlled manner this way, even if the growth rate is slow.

Oxide film deposition using ALD was tested on other porous materials next. Figure 9 displays data obtained from studies on the growth of aluminum oxide films on MCM-41, a silica-based solid with one-dimensional pores approximately 2.8 nm in diameter.[56] The smaller dimensions of these pores present a potential problem for ALD, as the mass transport inside the pores becomes difficult to control. This is highlighted by our results. The left panel of Figure 9 shows N_2 adsorption-desorption isotherms for MCM-41 before and after 2 Al_2O_3 ALD cycles. A few observations are worth highlighting from the data: (1) the isotherms show a much less marked

hysteresis loop than SBA-15, a reflection of an adsorption-desorption sequence closer to equilibrium and less affected by differences in capillary condensation versus capillary evaporation; (2) the main steep increase in volume uptake is seen at lower pressures than with SBA-15, a direct consequence of the smaller size of the pores; and (3) the ALD-treated sample actually shows two steps in the uptake, indicative of two pore sizes. This latter observation is more clearly seen in the pore size distributions calculated from these isotherms, which are shown in the right panel of Figure 9. Perhaps the most significant conclusion from that figure is the fact that the pore covering was only partial in these experiments, hence the bimodal pore size distribution seen after 2 ALD cycles. Unfortunately, increasing the TMA and/or H_2O exposure times in the ALD cycles, the way that better coverages were achieved with SBA-15, led mainly

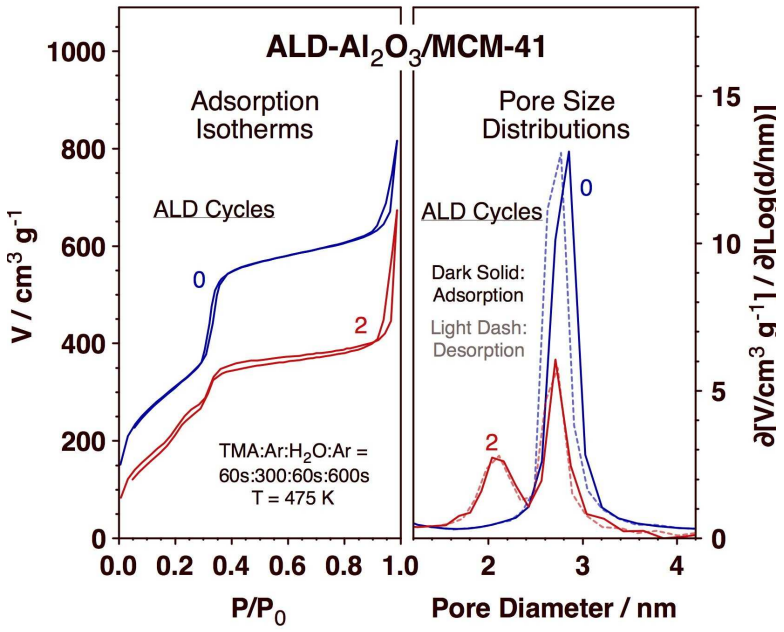

Figure 9. N_2 adsorption-desorption isotherms (left) and pore size distributions (right) from MCM-41 samples before and after 2 Al_2O_3 ALD cycles. Only partial pore coverage was attained in these experiments, highlighting the difficulties associated with ALD in small pores.

to further plugging of the pores (with the concomitant decreases in V and A) without any significant growth of the 2.1 nm diameter peak (data not shown). Increasing the reaction temperature seems to help minimize this plugging (by minimizing condensation inside the pores), but only to a limited extent (again, data not shown). Overall, it may be possible to deposit oxide films inside the pores of small-pore solids such as MCM-41, but that requires a much more careful design of the deposition process than with SBA-15 to solve the mass transport limitations.

Next, Al_2O_3 ALD experiments were carried on FDU-12, an ordered mesoporous material with a more complex pore structure consisting of large (> 10 nm in diameter) pores arranged in a 3D face-centered cubic (Fm-3m) arrangement and connected by small (< 4 nm in diameter) windows.[57] Typical characterization data for these samples are provided in Figure 10. Perhaps the most iconic difference between the adsorption-desorption isotherms from FDU-12 (shown in the left panel of Figure 10) and those of the other samples reported above is the marked asymmetry seen in the hysteresis loop, which with FDU-12 shows a very sharp drop in volume at relatively low pressures in the desorption branch. That is a reflection of the different dimensions associated with the diameters of the pores (which mainly affect the adsorption process) versus the windows (which limit the desorption); the corresponding size distributions are reported in the center and right panels, respectively. With our samples, the Al_2O_3 ALD reduces the inside volume of the pores, from an initial average diameter of approximately 20.6 nm (in a somewhat broad size distribution) to a value of 17.3 nm after 5 ALD cycles. In contrast, the size of the windows remains unmodified, at an average diameter of 3.8 nm.

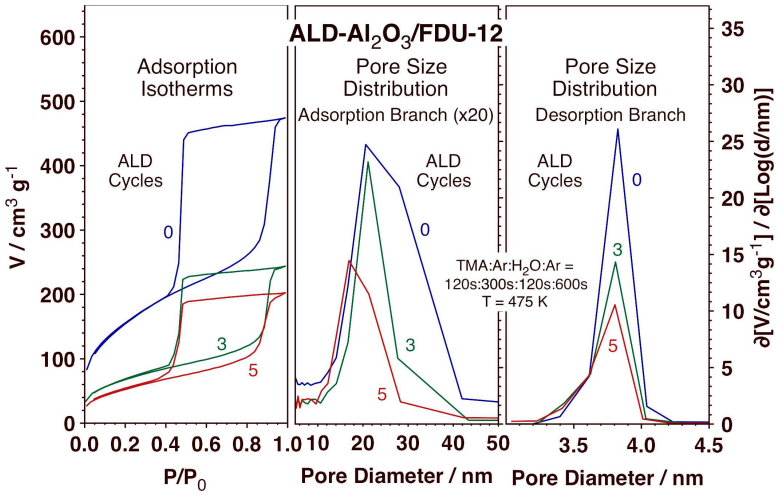

Figure 10. Characterization data for samples made by Al_2O_3 ALD on FDU-12 mesoporous materials. Left: N_2 adsorption-desorption isotherms for the FDU-12 as is and after 3 and 5 ALD cycles. Center: Pore size distributions, calculated from the adsorption branch. Right: Window size distributions, calculated from the desorption branch. Only the inside pore dimensions seem to be modified by the film growth.

Finally, the ALD of oxide films was tested on a typical porous silica material without structured pores, in our case spherical mesoporous silica particles (SMSP) made by typical sol-gel chemistry (the details are provided in the Experimental section). Typical data, for both the adsorption-desorption isotherms (left panel) and the calculated pore size distributions (right), are shown in Figure 11. In spite of the fact that these solid do not have well-defined pore structures, they still show relatively narrow distributions of pore sizes, around 2.7 nm in diameter for the pristine SMSP. Also, like with the MCM-41 samples, the small size of these pores means that the adsorption-desorption hysteresis is negligible, and that mass transport plays an important role in determining the final quality of the ALD films. Specifically, it is clear that the pore size distributions after Al_2O_3 ALD show bimodal, or even trimodal, diameter values: all samples retain some pores with 2.7 nm diameter, but develop new pores with 2.2 nm (2 Al_2O_3 ALD

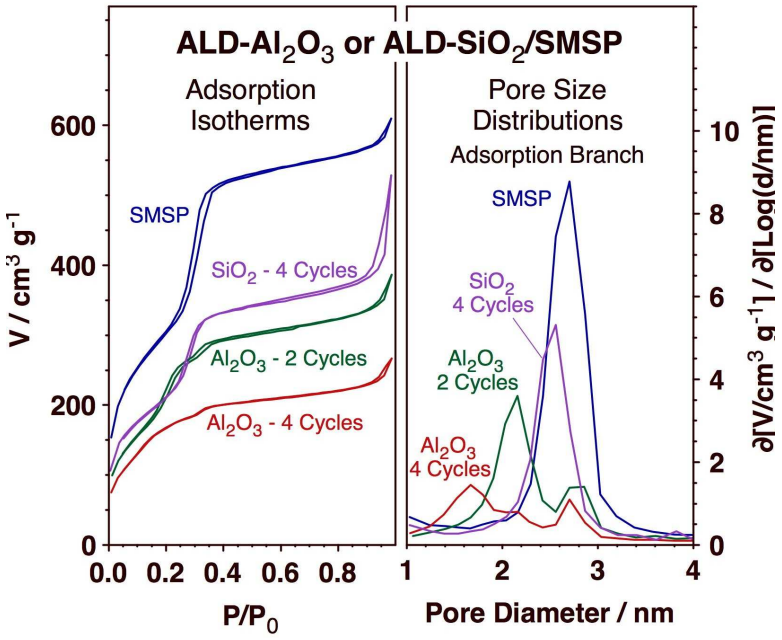

Figure 11. Characterization data for samples made by oxide ALD on spherical mesoporous silica particles (SMSP). Left: N_2 adsorption-desorption isotherms for the SMSP as is and after 2 and 4 Al_2O_3 ALD cycles and after 4 SiO_2 ALD cycles. Right: Pore size distributions calculated from the adsorption branch. Like with MCM-41, the small size of the pores leads to mass transport effects and to incomplete surface coverage, especially for the aluminum oxide deposition.

cycles) and 1.7 nm (4 Al_2O_3 cycles) diameters. With SiO_2 ALD, the deposition is much slower but the pores appear to be better covered: a unimodal pore size distribution is seen after 4 ALD cycles, with an average pore size of 2.55 nm.

4. Conclusions

The feasibility of growing thin oxide films on the surfaces of mesoporous materials by ALD was

systematically tested. Experiments were carried out to probe the deposition of aluminum oxide, titanium oxide, and silicon oxide on several substrates, SBA-15 and MCM-41, with linear 1D pores of well-defined diameters, FDU-12, which has large pores connected by small windows in a cubic 3D arrangement, and spherical mesoporous silica nanoparticles, where the pores are not as well structured. By using N_2 adsorption-desorption isotherms as the main probing tool, the characteristics of the mesopores were determined in terms of their geometrical parameters, namely, their pore size distributions, total pore volumes, and total surface areas, and used to optimize the ALD conditions. Good homogeneous films with narrow size distributions and homogeneous surface coverages could be deposited in most cases, but only after proper setting of the deposition conditions to avoid mass transport limitations. This was further corroborated by transmission electron microscopy.

On SBA-15, aluminum oxide and titanium oxide films can be easily deposited using TMA + H_2O and TDMAT + H_2O cycles, respectively. However, the ALD precursor exposure times, as well as the purging times, need to be tuned properly: long times and/or insufficient purging leads to condensation and subsequent pore plugging via CVD, whereas short times result in limited surface coverage, with the original silicon oxide surfaces of the back end of the pores left exposed. Tuning of the water exposure and reaction temperature was shown to be useful in optimizing the quality of the ALD as well. Silicon oxide deposition using TMOS + $NH_3 \cdot H_2O$, proved somewhat more difficult because of the slow nature of the chemistry involved. An alternative experimental setup was needed, and even with that arrangement deposition rates were slow.

ALD on the surfaces of small pores, such as those in MCM-41 or SMSP, is more difficult. Typically, bimodal pore size distributions, indicative of incomplete coverage, are observed, except perhaps with silicon oxide, where the slow nature of the deposition appears to help in terms of the final film quality. As opposed to the depositions on SBA-15, with MCM-41 or SMSP increasing the ALD precursor exposure time leads to pore plugging without helping much with surface coverage. More promising is the use of heat, as the processes at higher temperatures help minimize precursor condensation inside the pores. Finally, ALD on mesoporous materials with large cavities connected by small windows was shown to also be feasible. In that case, film deposition takes place inside the pores without altering the size of the windows.

Acknowledgements

Financial support for this project was provided by a grant from the U.S. Department of Energy, Office of Science, Basic Energy Sciences, Materials Sciences and Engineering (MSE) Division, under Award No. DE-FG02-03ER46599.

References

(1) George, S. M. Atomic Layer Deposition: An Overview. *Chem. Rev.* **2010**, *110*, 111-131.

(2) Zaera, F. Mechanisms of Surface Reactions in Thin Solid Film Chemical Deposition Processes. *Coord. Chem. Rev.* **2013**, *257*, 3177-3191.

(3) Hämäläinen, J.; Ritala, M.; Leskelä, M. Atomic Layer Deposition of Noble Metals and Their Oxides. *Chem. Mater.* **2014**, *26*, 786-801.

(4) Lu, J.; Elam, J. W.; Stair, P. C. Atomic Layer Deposition—Sequential Self-Limiting Surface Reactions for Advanced Catalyst "Bottom-up" Synthesis. *Surf. Sci. Rep.* **2016**, *71*, 410-472.

(5) Kim, H. Atomic Layer Deposition of Metal and Nitride Thin Films: Current Research Efforts and Applications for Semiconductor Device Processing. *J. Vac. Sci. Technol. B* **2003**, *21*, 2231-2261.

(6) Schumacher, M.; Baumann, P. K.; Seidel, T. Avd and ALD as Two Complementary Technology Solutions for Next Generation Dielectric and Conductive Thin-Film Processing. *Chem. Vap. Deposition* **2006**, *12*, 99-108.

(7) Niinistö, J.; Kukli, K.; Heikkilä, M.; Ritala, M.; Leskelä, M. Atomic Layer Deposition of High-k Oxides of the Group 4 Metals for Memory Applications. *Adv. Eng. Mater.* **2009**, *11*, 223-234.

(8) Kim, H.; Lee, H.-B.-R.; Maeng, W. J. Applications of Atomic Layer Deposition to Nanofabrication and Emerging Nanodevices. *Thin Solid Films* **2009**, *517*, 2563-2580.

(9) Putkonen, M. ALD Applications Beyond Outside IC Technology- Existing and Emerging Possibilities. *ECS Trans.* **2009**, *25*, 143-155.

(10) Meng, X.; Yang, X.-Q.; Sun, X. Emerging Applications of Atomic Layer Deposition for Lithium-Ion Battery Studies. *Adv. Mater.* **2012**, *24*, 3589-3615.

(11) Delft, J. A. v.; Garcia-Alonso, D.; Kessels, W. M. M. Atomic Layer Deposition for Photovoltaics: Applications and Prospects for Solar Cell Manufacturing. *Semicond. Sci. Technol.* **2012**, *27*, 074002.

(12) Johnson, R. W.; Hultqvist, A.; Bent, S. F. A Brief Review of Atomic Layer Deposition: From Fundamentals to Applications. *Mater. Today* **2014**, *17*, 236-246.

(13) Sobel, N.; Hess, C. Nanoscale Structuring of Surfaces by Using Atomic Layer Deposition. *Angew. Chem., Int. Ed.* **2015**, *54*, 15014-15021.

(14) Meng, X.; Wang, X.; Geng, D.; Ozgit-Akgun, C.; Schneider, N.; Elam, J. W. Atomic Layer Deposition for Nanomaterial Synthesis and Functionalization in Energy Technology. *Mater. Horiz.* **2017**, *4*, 133-154.

(15) Sharma, K.; Routkevitch, D.; Varaksa, N.; George, S. M. Spatial Atomic Layer Deposition on Flexible Porous Substrates: ZnO on Anodic Aluminum Oxide Films and Al_2O_3 on Li Ion Battery Electrodes. *J. Vac. Sci. Technol., A* **2016**, *34*, 01A146.

(16) Gordon, R. G.; Hausmann, D.; Kim, E.; Shepard, J. A Kinetic Model for Step Coverage by Atomic Layer Deposition in Narrow Holes or Trenches. *Chem. Vap. Deposition* **2003**, *9*, 73-78.

(17) Elam, J. W.; Routkevitch, D.; Mardilovich, P. P.; George, S. M. Conformal Coating on Ultrahigh-Aspect-Ratio Nanopores of Anodic Alumina by Atomic Layer Deposition. *Chem. Mater.* **2003**, *15*, 3507-3517.

(18) Dendooven, J.; Deduytsche, D.; Musschoot, J.; Vanmeirhaeghe, R. L.; Detavernier, C. Modeling the Conformality of Atomic Layer Deposition: The Effect of Sticking

Probability. *J. Electrochem. Soc.* **2009**, *156*, P63-P67.

(19) Rose, M.; Bartha, J. W. Method to Determine the Sticking Coefficient of Precursor Molecules in Atomic Layer Deposition. *Appl. Surf. Sci.* **2009**, *255*, 6620-6623.

(20) Keuter, T.; Menzler, N. H.; Mauer, G.; Vondahlen, F.; Vaßen, R.; Buchkremer, H. P. Modeling Precursor Diffusion and Reaction of Atomic Layer Deposition in Porous Structures. *J. Vac. Sci. Technol., A* **2015**, *33*, 01A104.

(21) Lankhorst, A. M.; Paarhuis, B. D.; Terhorst, H. J. C. M.; Simons, P. J. P. M.; Kleijn, C. R. Transient ALD Simulations for a Multi-Wafer Reactor with Trenched Wafers. *Surf. Coat. Technol.* **2007**, *201*, 8842-8848.

(22) Mahurin, S.; Bao, L.; Yan, W.; Liang, C.; Dai, S. Atomic Layer Deposition of TiO_2 on Mesoporous Silica. *J. Non-Cryst. Solids* **2006**, *352*, 3280-3284.

(23) Detavernier, C.; Dendooven, J.; Pulinthanathu Sree, S.; Ludwig, K. F.; Martens, J. A. Tailoring Nanoporous Materials by Atomic Layer Deposition. *Chem. Soc. Rev.* **2011**, *40*, 5242-5253.

(24) Cassidy David, E.; DeSisto William, J. Atomic Layer Deposition‐Modified Ordered Mesoporous Silica Membranes. *Chem. Vap. Deposition* **2012**, *18*, 22-26.

(25) Zemtsova, E. G.; Arbenin, A. Y.; Plotnikov, A. F.; Smirnov, V. M. Pore Radius Fine Tuning of a Silica Matrix (MCM-41) Based on the Synthesis of Alumina Nanolayers with Different Thicknesses by Atomic Layer Deposition. *J. Vac. Sci. Technol., A* **2015**, *33*, 021519.

(26) Sun, X.; Xie, M.; Wang, G.; Sun, H.; Cavanagh, A. S.; Travis, J. J.; George, S. M.; Lian, J. Atomic Layer Deposition of TiO_2 on Graphene for Supercapacitors. *J. Electrochem. Soc.* **2012**, *159*, A364-A369.

(27) Sun, X.; Zhou, C.; Xie, M.; Sun, H.; Hu, T.; Lu, F.; Scott, S. M.; George, S. M.; Lian, J. Synthesis of ZnO Quantum Dot/Graphene Nanocomposites by Atomic Layer Deposition with High Lithium Storage Capacity. *Journal of Materials Chemistry A* **2014**, *2*, 7319-7326.

(28) Zaera, F. Nanostructured Materials for Applications in Heterogeneous Catalysis. *Chem. Soc. Rev.* **2013**, *42*, 2746-2762.

(29) Lu, J.; Elam, J. W.; Stair, P. C. Synthesis and Stabilization of Supported Metal Catalysts by Atomic Layer Deposition. *Acc. Chem. Res.* **2013**, *46*, 1806-1815.

(30) O'Neill, B. J.; Jackson, D. H. K.; Crisci, A. J.; Farberow, C. A.; Shi, F.; Alba-Rubio, A. C.; Lu, J.; Dietrich, P. J.; Gu, X.; Marshall, C. L.et al. Stabilization of Copper Catalysts for Liquid-Phase Reactions by Atomic Layer Deposition. *Angew. Chem., Int. Ed.* **2013**, *52*, 13808-13812.

(31) Zaera, F. Shape-Controlled Nanostructures in Heterogeneous Catalysis. *ChemSusChem* **2013**, *6*, 1797-1820.

(32) Pagán-Torres, Y. J.; Lu, J.; Nikolla, E.; Alba-Rubio, A. C. Well-Defined Nanostructures for Catalysis by Atomic Layer Deposition. *Stud. Surf. Sci. Catal.* **2017**, *177*, 643-676.

(33) Singh, J. A.; Yang, N.; Bent, S. F. Nanoengineering Heterogeneous Catalysts by Atomic Layer Deposition. *Annu. Rev. Chem. Biomol. Eng.* **2017**, *8*, 41-62.

(34) Weng, Z.; Zaera, F. Sub-Monolayer Control of Mixed-Oxide Support Composition in Catalysts via Atomic Layer Deposition: Selective Hydrogenation of Cinnamaldehyde Promoted by (SiO_2-ALD)-Pt/Al_2O_3. *ACS Catal.* **2018**, DOI: 10.1021/acscatal.1028b02431.

(35) Puurunen, R. L. Surface Chemistry of Atomic Layer Deposition: A Case Study for the

Trimethylaluminum/Water Process. *J. Appl. Phys.* **2005**, *97*, 121301.

(36) Wind, R. A.; George, S. M. Quartz Crystal Microbalance Studies of Al_2O_3 Atomic Layer Deposition Using Trimethylaluminum and Water at 125 °C. *J. Phys. Chem. A* **2009**, *114*, 1281-1289.

(37) Sree, S. P.; Dendooven, J.; Koranyi, T. I.; Vanbutsele, G.; Houthoofd, K.; Deduytsche, D.; Detavernier, C.; Martens, J. A. Aluminium Atomic Layer Deposition Applied to Mesoporous Zeolites for Acid Catalytic Activity Enhancement. *Catal. Sci. Technol.* **2011**, *1*, 218-221.

(38) Feng, H.; Lu, J.; Stair, P.; Elam, J. Alumina over-Coating on Pd Nanoparticle Catalysts by Atomic Layer Deposition: Enhanced Stability and Reactivity. *Catal. Lett.* **2011**, *141*, 512-517.

(39) Lim, G. T.; Kim, D. H. Characteristics of TiO_x Films Prepared by Chemical Vapor Deposition Using Tetrakis-Dimethyl-Amido-Titanium and Water. *Thin Solid Films* **2006**, *498*, 254-258.

(40) Xie, Q.; Jiang, Y. L.; Detavernier, C.; Deduytsche, D.; Van Meirhaeghe, R. L.; Ru, G. P.; Li, B. Z.; Qu, X. P. Atomic Layer Deposition of TiO_2 from Tetrakis-Dimethyl-Amido Titanium or Ti Isopropoxide Precursors and H_2O. *J. Appl. Phys.* **2007**, *102*.

(41) Abendroth, B.; Moebus, T.; Rentrop, S.; Strohmeyer, R.; Vinnichenko, M.; Weling, T.; Stöcker, H.; Meyer, D. C. Atomic Layer Deposition of TiO_2 from Tetrakis(Dimethylamino)Titanium and H_2O. *Thin Solid Films* **2013**, *545*, 176-182.

(42) Zhuiykov, S.; Akbari, M. K.; Hai, Z.; Xue, C.; Xu, H.; Hyde, L. Wafer-Scale Fabrication of Conformal Atomic-Layered TiO2 by Atomic Layer Deposition Using Tetrakis (Dimethylamino) Titanium and H_2O Precursors. *Materials & Design* **2017**, *120*, 99-108.

(43) Kern, W.; Rosler, R. S. Advances in Deposition Processes for Passivation Films. *J. Vac. Sci. Technol.* **1977**, *14*, 1082-1099.

(44) Hatton, B.; Kitaev, V.; Perovic, D.; Ozin, G.; Aizenberg, J. Low-Temperature Synthesis of Nanoscale Silica Multilayers - Atomic Layer Deposition in a Test Tube. *J. Mater. Chem.* **2010**, *20*, 6009-6013.

(45) Klaus, J. W.; George, S. M. Atomic Layer Deposition of SiO_2 at Room Temperature Using NH_3-Catalyzed Sequential Surface Reactions. *Surf. Sci.* **2000**, *447*, 81-90.

(46) Ferguson, J. D.; Smith, E. R.; Weimer, A. W.; George, S. M. ALD of SiO_2 at Room Temperature Using Teos and H_2O with NH_3 as the Catalyst. *J. Electrochem. Soc.* **2004**, *151*, G528-G535.

(47) Kim, M. S.; Jeon, J. B.; Chang, J. Y. Selectively Functionalized Mesoporous Silica Particles with the Pegylated Outer Surface and the Doxorubicin-Grafted Inner Surface: Improvement of Loading Content and Solubility. *Microporous Mesoporous Mater.* **2013**, *172*, 118-124.

(48) Barrett, E. P.; Joyner, L. G.; Halenda, P. P. The Determination of Pore Volume and Area Distributions in Porous Substances. I. Computations from Nitrogen Isotherms. *J. Am. Chem. Soc.* **1951**, *73*, 373-380.

(49) Sing, K. S. W.; Everett, D. H.; Haul, R. A. W.; Moscou, L.; Pierotti, R. A.; Rouquerol, J.; Siemieniewska, T. Reporting Physisorption Data for Gas/Solid Systems with Special Reference to the Determination of Surface Area and Porosity. *Pure Appl. Chem.* **1985**, *57*, 603-619.

(50) Brunauer, S.; Emmett, P. H.; Teller, E. Adsorption of Gases in Multimolecular Layers. *J. Am. Chem. Soc.* **1938**, *60*, 309-319.

(51) Groner, M. D.; Fabreguette, F. H.; Elam, J. W.; George, S. M. Low-Temperature Al_2O_3 Atomic Layer Deposition. *Chem. Mater.* **2004**, *16*, 639-645.

(52) Elam, J. W.; Libera, J. A.; Huynh, T. H.; Feng, H.; Pellin, M. J. Atomic Layer Deposition of Aluminum Oxide in Mesoporous Silica Gel. *J. Phys. Chem. C* **2010**, *114*, 17286-17292.

(53) Jambhrunkar, S.; Yu, M.; Yang, J.; Zhang, J.; Shrotri, A.; Endo-Munoz, L.; Moreau, J.; Lu, G.; Yu, C. Stepwise Pore Size Reduction of Ordered Nanoporous Silica Materials at Angstrom Precision. *J. Am. Chem. Soc.* **2013**, *135*, 8444-8447.

(54) Ruff, P.; Lauterbach, S.; Kleebe, H.-J.; Hess, C. Surface Structuring of Mesoporous Materials by Controlled Synthesis of Nanocavities. *Microporous Mesoporous Mater.* **2016**, *235*, 160-169.

(55) Li, Y.; Zhao, S.; Hu, Q.; Gao, Z.; Liu, Y.; Zhang, J.; Qin, Y. Highly Efficient Coo_x/SBA-15 Catalysts Prepared by Atomic Layer Deposition for the Epoxidation Reaction of Styrene. *Catal. Sci. Technol.* **2017**, *7*, 2032-2038.

(56) Beck, J. S.; Vartuli, J. C.; Roth, W. J.; Leonowicz, M. E.; Kresge, C. T.; Schmitt, K. D.; Chu, C. T. W.; Olson, D. H.; Sheppard, E. W. A New Family of Mesoporous Molecular Sieves Prepared with Liquid Crystal Templates. *J. Am. Chem. Soc.* **1992**, *114*, 10834-10843.

(57) Fan, J.; Yu, C.; Gao, F.; Lei, J.; Tian, B.; Wang, L.; Luo, Q.; Tu, B.; Zhou, W.; Zhao, D. Cubic Mesoporous Silica with Large Controllable Entrance Sizes and Advanced Adsorption Properties. *Angew. Chem., Int. Ed.* **2003**, *42*, 3146-3150.

TOC Statement:

Mixed oxide surfaces were developed via the atomic layer deposition of a variety of oxide thin films on mesoporous materials.